

Towards Adversarial Robustness via Debiased High-Confidence Logit Alignment

Kejia Zhang¹, Juanjuan Weng^{2*}, Shaozi Li¹, Zhiming Luo^{1,3}

¹Department of Artificial Intelligence, Xiamen University, Xiamen, China

²College of Information Science and Technology, Jinan University, Guangzhou, China

³Key Laboratory of Multimedia Trusted Perception and Efficient Computing, Ministry of Education of China, Xiamen University

kejiaz171@gmail.com, jjweng@jnu.edu.cn, {szlig, zhiming.luo}@xmu.edu.cn

Abstract

Despite the remarkable progress of deep neural networks (DNNs) in various visual tasks, their vulnerability to adversarial examples raises significant security concerns. Recent adversarial training methods leverage inverse adversarial attacks to generate high-confidence examples, aiming to align adversarial distributions with high-confidence class regions. However, our investigation reveals that under inverse adversarial attacks, high-confidence outputs are influenced by biased feature activations, causing models to rely on background features that lack a causal relationship with the labels. This spurious correlation bias leads to overfitting irrelevant background features during adversarial training, thereby degrading the model's robust performance and generalization capabilities. To address this issue, we propose *Debiased High-Confidence Adversarial Training (DHAT)*, a novel approach that aligns adversarial logits with debiased high-confidence logits and restores proper attention by enhancing foreground logit orthogonality. Extensive experiments demonstrate that DHAT achieves state-of-the-art robustness on both CIFAR and ImageNet-1K benchmarks, while significantly improving generalization by mitigating the feature bias inherent in inverse adversarial training approaches. Code is available at <https://github.com/KejiaZhang-Robust/DHAT>.

1. Introduction

Deep neural networks (DNNs) have demonstrated exceptional performance across a range of visual tasks [13, 26, 37, 53]. However, these networks remain susceptible to adversarial attacks, which present significant security challenges [11, 42]. Adversarial attacks introduce subtle perturbations that are imperceptible to humans but can significantly disrupt the inference process of DNNs, leading to incorrect predictions. Adversarial training (AT) is widely rec-

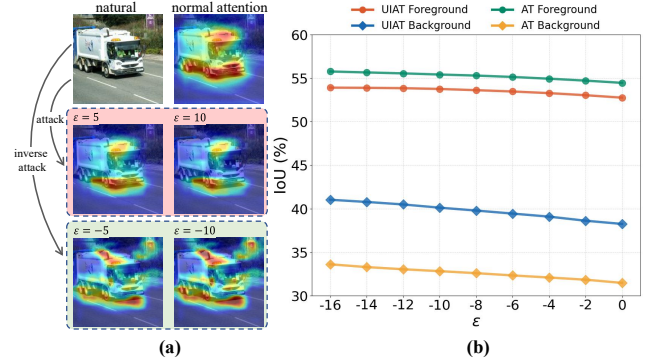


Figure 1. Inverse adversarial attack exploits spurious correlations via attention misallocation to non-causal background features. The negative ϵ denotes inverse adversarial perturbation strength. (a) Grad-CAM [34] visualizations show that adversarial attacks disrupt attention and cause errors, while inverse adversarial attacks amplify activation and improve accuracy but expose a critical flaw: attention shifts from foreground to irrelevant background regions. (b) Quantitative comparison of IoU(%) between attention regions and the true foreground and background regions using UIAT [9] and AT. Increasing inverse attack strength $-\epsilon$ demonstrates UIAT's disproportionate focus on non-causal background features, exposing reliance on spurious correlations [3, 30, 35].

ognized as one of the most effective methods for defending against these attacks by incorporating adversarial examples into the training process [14, 36].

Recently, numerous advanced AT-based techniques have been proposed to address the vulnerabilities of DNNs [19, 24, 25, 40]. Prominent methods in this domain focus on aligning the distributions of adversarial examples to their true classes, thereby enhancing classification accuracy under adversarial attacks. For example, MART [45] and TRADES [54] aim to align the logits of adversarial examples with their corresponding natural examples, promoting consistency in predictions. Expanding on this, UIAT [9] and ACR [5] extend this approach by generating inverse adversarial examples [32] that exhibit higher confidence compared to their natural counterparts. This strategy helps al-

*Corresponding author

leviate the negative impact of misclassification of natural examples in alignment and directs adversarial examples toward regions with correct high-confidence classifications.

Upon investigation, we uncover a **remarkable yet concerning phenomenon**: inverse adversarial examples produce high-confidence outputs by triggering biased feature activation. To illuminate this effect, we visualize attention maps from a conventional adversarial training (AT) model under both adversarial and inverse adversarial attacks (see Figure 1 (a)). Adversarial attacks disrupt normal attention patterns, causing incorrect predictions. In contrast, inverse adversarial attacks amplify the model’s attention on features, with stronger attacks even improving prediction accuracy [9, 48]. However, this apparent enhancement masks a **critical flaw**: the model’s attention systematically shifts from discriminative foreground features to irrelevant background regions—akin to identifying a sheep by detecting grass rather than the animal itself. This reliance on spurious correlations undermines the model’s causal reasoning capabilities and compromises its robustness [1, 6, 20].

To delve deeper into this issue, we conduct a **statistical analysis** using the Intersection over Union (IoU) metric to measure the alignment between attention maps and foreground/background regions on a subset of ImageNet [18]. Leveraging the Class Activation Mapping (CAM)-based technique inspired by [10], we define foreground as regions with high-class activation (*i.e.*, areas critical for predictions) and background as regions with low activation. Comparing the UIAT model [9] (trained with inverse adversarial examples) to a standard AT model reveals a **concerning trend**. As evidenced in Figure 1 (b), while increasing the magnitude ϵ of inverse adversarial attacks enhances overall feature attention, the UIAT model fails to improve IoU for foreground features compared to the AT model. Instead, it demonstrates a marked increase in IoU for background features—a clear indicator of attention misallocation.

This leads to a **pivotal insight**: the inverse adversarial training disproportionately skews attention toward background features, resulting in biased feature activation. This shift engenders a **fundamental vulnerability**: a spurious correlation bias where the model becomes overly dependent on contextual background cues rather than intrinsic object features. Much like a classifier that associates beaches with birds rather than wings and beaks, this misplaced reliance significantly degrades robustness and generalization performance [15, 55], as conclusively demonstrated in Table 5.

Building upon the above findings, we introduce a method named Debiased High-Confidence Adversarial Training (DHAT). DHAT implements two key techniques: Debiased High-Confidence Logit Regularization (DHLR) and Foreground Logit Orthogonal Enhancement (FLOE). DHLR quantifies the bias towards background feature activation and debias the spurious correlations by recalibrating the

biased high-confidence logits derived from inverse adversarial examples. This regularization aligns the logits of adversarial examples with debiased high-confidence logits to improve adversarial robustness and mitigate spurious correlation bias. FLOE further refines this process by reducing the correlation between high-confidence logits and background features in affine space, which helps restore the model’s attention to its normal state. Extensive experiments demonstrate that DHAT outperforms state-of-the-art techniques across various datasets, providing superior adversarial robustness and generalization. Additionally, our DHAT can be seamlessly integrated with existing advanced adversarial training methods.

Below, we outline our principal contributions:

- We identify that the adversarial training model shows a biased feature activation under inverse adversarial attacks. Training with inverse adversarial examples causes the model’s attention shifting towards background features, thus lead to spurious correlation bias.
- We introduce a novel method, Debiased High-Confidence Adversarial Training (DHAT). This method aligns the logits of adversarial examples with debiased high-confidence logits corresponding to their classes, effectively mitigating spurious correlation bias.
- Extensive experiments validate the superior robustness and generalization of our method against adversarial attacks. Additionally, our approach integrates smoothly with existing advanced adversarial training strategies.

2. Related Work

2.1. Adversarial Attack

Adversarial attacks introduce subtle perturbations δ into natural examples x , causing DNNs to produce incorrect predictions rather than the true class y . These attacks are typically formulated as an optimization problem:

$$\hat{x} = \max_{\|\delta\|_p \leq \epsilon} (\mathcal{L}_{\text{attack}}(\theta; x + \delta, y)), \quad (1)$$

where \hat{x} represents the adversarial example, $\mathcal{L}_{\text{attack}}$ is the adversarial attack loss function, θ denotes the model parameters, and δ is constrained to the p -norm ball of radius ϵ .

Numerous studies have investigated the vulnerability of DNNs and have proposed various adversarial attack methods. Goodfellow et al. [14] introduced the Fast Gradient Sign Method (FGSM), which compute the adversarial perturbation in the direction of the gradient:

$$\delta = \eta \cdot \text{sign}(\nabla_x \mathcal{L}_{\text{attack}}(\theta; x, y)), \quad (2)$$

where η denotes the attack step size. Building on this, Madry et al. [29] proposed Projected Gradient Descent (PGD), which iteratively updates the gradient of the input

data to generate more potent adversarial examples, thereby increasing the success rate of attacks:

$$\hat{x}^{t+1} = \Pi_{\mathbb{B}(\epsilon)}\{\hat{x}^t + \eta \cdot \text{sign}(\nabla_{\hat{x}^t} \mathcal{L}_{\text{attack}}(\theta; \hat{x}^t, y))\}, \quad (3)$$

where $\Pi_{\mathbb{B}(\epsilon)}$ projects the perturbation onto the p -norm ball of radius ϵ . Furthermore, Carlini and Wagner [4] developed the Carlini-Wagner (C&W) attack, an optimization-based method capable of producing more imperceptible adversarial examples. Croce and Hein [7] introduced AutoAttack, an ensemble attack strategy that is user-independent and parameter-free.

2.2. Adversarial Defense

Adversarial training (AT) is a widely used strategy for improving model robustness. The core principle of AT is to include adversarial examples in the training process, thereby aligning the model’s outputs towards the true label distribution [12, 50]. Mathematically, conventional AT methods are formulated as a min-max optimization problem:

$$\min_{\theta} \mathbb{E}_{(x,y) \sim \mathcal{D}} \max_{\|\delta\|_p \leq \epsilon} \mathcal{L}_{AT}(\theta; \mathcal{G}_{\theta}(x, \delta), y), \quad (4)$$

where (x, y) denotes a clean image-label pair sampled from the data distribution \mathcal{D} , δ is constrained to the maximum p -norm magnitude ϵ , \mathcal{L}_{AT} represents the training strategy function, and $\mathcal{G}_{\theta}(x, \delta)$ denotes the attack generation procedure incorporating the perturbation δ . The outer minimization optimizes the model parameters θ to minimize the expected loss over adversarial examples, while the inner maximization identifies the perturbations that maximize this loss, thereby enhancing the model’s robustness.

Recent advancements in AT have introduced several techniques to further improve adversarial robustness. Wu et al. [49] introduced Adversarial Weight Perturbation (AWP), which enhances robustness by flattening the loss landscape with respect to input variations. Kim et al. [21] proposed Feature Separation and Recalibration (FSR) to capture useful logits from non-robust features. Wei et al. [47] developed Class-wise Calibrated Fair Adversarial Training (CFA), which adaptively configures training for each class to achieve category-level robust fairness. Li et al. [27] proposed SGLR, which uses self-distillation to refine the soft-label distribution logits, thereby calibrating the adversarial training.

Methods similar to our approach include MART [45] and UIAT [9]. These methods use Kullback-Leibler (KL) divergence to align the logits of adversarial examples with high-confidence logits. MART encourages sharing a similar logit distribution between adversarial examples and their corresponding natural examples. UIAT generates inverse adversarial examples [32] that exhibit higher confidence compared to natural examples, thereby enhancing the alignment of adversarial examples towards the high-confidence regions of the decision surface.

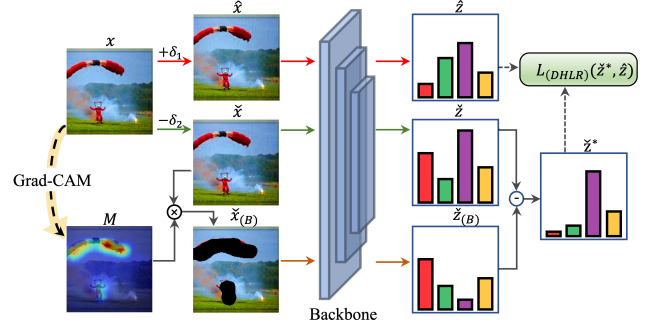


Figure 2. Overview of Debiased High-Confidence Logits Regularization (DHLR). The method first quantifies the degree of biased activation towards background features and recalibrates biased logits, then aligns the logits of adversarial examples with debiased high-confidence logits.

3. Methodology

In this section, we introduce the basic notation and present our approach to mitigate adversarial bias and improve robustness. Our method recalibrates high-confidence logits and reduces reliance on spurious background features. The optimization strategy is outlined, with pseudocode provided in Section 7 of the supplementary material.

3.1. Notation

We denote the training dataset as $(X, Y) = \{(x_i, y_i) \mid i \in (1, 2, \dots, N)\}$, where x and y denote the natural input examples and their corresponding labels, respectively. N represents the total number of examples in the dataset. Let θ denote the parameters of a convolutional neural network (CNN) for image classification. The network’s output logits are denoted as $f_{\theta}(\cdot)$, and the final predicted label is given by $\arg \max f_{\theta}(\cdot)$. Inverse adversarial examples \tilde{x} can be regarded as examples for which the model correctly predicts the label with high-confidence. These examples are generated by applying image perturbations aimed at minimizing the attack loss [32]:

$$\tilde{x} = \min_{\|\delta\|_p \leq \epsilon} (\mathcal{L}_{\text{Inv}}(\theta; x - \delta, y)), \quad (5)$$

where \mathcal{L}_{Inv} denotes the loss function used to generate inverse adversarial attack. The logits of the inverse adversarial example \tilde{x} and the adversarial example \hat{x} are computed as $\tilde{z} = f_{\theta}(\tilde{x})$ and $\hat{z} = f_{\theta}(\hat{x})$, respectively.

3.2. Debiased High-Confidence Logit Regularization

To mitigate the spurious correlation bias introduced by adversarial training with inverse adversarial examples, we propose utilizing debiased high-confidence logits for regularization. Specifically, this approach involves separating and

quantifying the spurious bias towards background features under inverse adversarial attacks, and then recalibrating the biased high-confidence logits to align with those of adversarial examples, as illustrated in Figure 2.

First, we quantify the model’s biased activation degree towards background features under inverse adversarial attacks. Following the approach proposed by [10], we use using Grad-CAM [33] or alternative methods such as SAM [22] to generate pixel-wise attention maps $M \in [0, 1]^{n \times n}$ for the natural example x . We separate the background feature $\tilde{x}_{(B)}$ from the inverse adversarial examples \tilde{x} based on the M :

$$[\tilde{x}_{(B)}]_{(i,j)} = \mathbb{I}_{(M_{i,j} < \omega)} \cdot \tilde{x}_{(i,j)}, \quad (6)$$

where $\mathbb{I}_{(M_{i,j} < \omega)}$ is an indicator function and ω is a predefined threshold. Next, we compute the logits for the background feature $\tilde{x}_{(B)}$:

$$\tilde{z}_{(B)} = f_{\theta}(\tilde{x}_{(B)}). \quad (7)$$

These logits can quantify the biased degree introduced by background feature activation during network inference.

To recalibrate the biased high-confidence logits, we refine the logits of inverse adversarial examples by subtracting the background feature logits:

$$\tilde{z}^* = \tilde{z} - \tilde{z}_{(B)}, \quad (8)$$

where \tilde{z}^* represents the debiased high-confidence logits.

Next, we introduce a regularizer to align the logits of adversarial examples with these debiased high-confidence logits. This regularization encourages the model to focus on foreground features and mitigates the biased activation of background features. Specifically, our Debiased High-Confidence Logit Regularization (DHLR) is defined as:

$$\mathcal{L}_{DHLR}(\tilde{z}^*, \hat{z}) = \mathcal{L}_{KL}(\phi(\tilde{z}^*) || \phi(\hat{z})), \quad (9)$$

where ϕ denotes the softmax function, \mathcal{L}_{KL} represents the Kullback–Leibler (KL) divergence.

This regularization term \mathcal{L}_{DHLR} promotes consistency between the logits of adversarial examples \hat{z} and the debiased high-confidence logits \tilde{z}^* . This alignment mitigates spurious correlation bias, thereby improving adversarial robustness and generalization.

3.3. Foreground Logit Orthogonal Enhancement

While DHLR effectively recalibrates high-confidence logits to mitigate spurious correlations, it fails to fully restore the model’s focus on foreground features when handling inverse adversarial examples \tilde{x} . This is because DHLR primarily aligns logits with debiased high-confidence targets, without directly addressing the model’s persistent bias toward background features. Under inverse adversarial attacks, the model still exhibits strong activation in irrelevant background regions, undermining its ability to prioritize critical foreground cues.

To address this issue, we introduce Foreground Logit Orthogonal Enhancement (FLOE), a targeted method designed to minimize the correlation between high-confidence logits \tilde{z} and background feature logits $\tilde{z}_{(B)}$. The intuition behind FLOE is straightforward: by reducing the projection of \tilde{z} onto $\tilde{z}_{(B)}$ in the affine space, we make \tilde{z} less explainable by $\tilde{z}_{(B)}$, thereby encouraging the model to rely more on foreground features. This projection-based approach ensures that the model’s predictions are driven by meaningful foreground information rather than spurious background correlations. The optimization objective is formulated as:

$$\mathcal{L}_{FLOE}(\tilde{z}, \tilde{z}_{(B)}) = -|\tilde{z} - \frac{\tilde{z} \cdot \tilde{z}_{(B)}}{|\tilde{z}_{(B)}|^2} \cdot \tilde{z}_{(B)}|_p, \quad (10)$$

where p indicates the norm exponent. The term \mathcal{L}_{FLOE} is designed to alleviate biased feature activation under inverse adversarial attacks.

3.4. Optimization Strategy

Finally, we integrate the DHLR and FLOE techniques into a unified training framework Debiased High-Confidence Adversarial Training (DHAT). The overall optimization objective for DHAT is formulated as:

$$\mathcal{L}_{DHAT} = \mathcal{L}_{AT}(\hat{z}, y) + \lambda_1 \cdot \mathcal{L}_{DHLR}(\tilde{z}^*, \hat{z}) + \lambda_2 \cdot \mathcal{L}_{FLOE}(\tilde{z}, \tilde{z}_{(B)}), \quad (11)$$

where $\mathcal{L}_{AT}(\hat{z}, y)$ represents the standard adversarial training loss, and λ_1 and λ_2 are hyperparameters that control the relative contributions of the DHLR and FLOE terms, respectively. Besides, our DHAT can be seamlessly integrated with various advanced adversarial training strategies represented by \mathcal{L}_{AT} to improve the robustness.

4. Experiments

4.1. Experimental Settings

4.1.1. Datasets and models.

We conduct experiments on the CIFAR-10, CIFAR-100 [23], and ImageNet-1K [31] datasets. The architecture for our experiments include the mainstream models WRN28-10 [52], ResNet-18 [16], ResNet-50 [16], Inception-V3 [43], and VGG16 [38]. Detailed information is provided in the supplementary material.

4.1.2. Training setup

For CIFAR datasets, each model is trained for 100 epochs, with the learning rate reduced by a factor of 0.1 at the 80th and 90th epochs. For adversarial example generation, we use a fixed 10-iteration attack. The maximum ℓ_{∞} -norm of the adversarial perturbation is set to $\epsilon = 8/255$, while the inverse adversarial perturbation is set to $\epsilon = 4/255$. Both perturbations use a fixed step size of $\alpha = 2/255$. For the

Table 1. Comparison of robustness (%) and robust generalization gap (%). The **number** in bold indicates the best performance.

Architecture: WRN28-10		Attack ($\epsilon = 4/255$)					Robust Gap↓
ImageNet-1K	Clean↑	PGD-10↑	PGD-20↑	PGD-50↑	C&W↑	AA↑	
MART [45]	62.31	43.56	42.89	42.54	40.62	38.94	13.76
AWP [49]	64.25	45.13	44.67	44.21	41.96	40.02	12.82
FSR [21]	64.70	44.31	43.82	43.45	41.23	39.30	14.17
CFA [47]	65.38	44.87	44.32	43.96	41.58	39.65	15.49
UIAT [9]	62.64	45.29	44.85	44.57	42.13	40.18	14.68
SGLR [27]	63.46	44.52	44.05	43.78	41.36	39.47	19.72
DHAT (Ours)	65.90	46.83	46.42	46.11	43.25	41.70	9.53
DHAT-AWP (Ours)	65.62	47.38	47.04	46.79	43.62	42.07	10.27
DHAT-CFA (Ours)	66.26	48.27	47.89	47.53	44.18	42.45	11.64

Architecture: WRN28-10		Attack ($\epsilon = 8/255$)					Robust Gap↓
CIFAR-10	Clean↑	PGD-10↑	PGD-20↑	PGD-50↑	C&W↑	AA↑	
MART [45]	82.99	56.25	55.48	55.45	52.26	50.67	9.52
AWP [49]	82.67	57.80	57.21	57.07	54.82	51.90	6.90
FSR [21]	82.92	56.69	55.94	55.51	53.93	51.74	7.42
CFA [47]	84.43	57.87	56.90	56.64	54.60	51.85	10.36
UIAT [9]	82.94	58.66	58.12	58.05	54.11	52.17	7.92
SGLR [27]	85.76	57.53	56.91	56.66	54.28	52.07	9.38
DHAT (Ours)	83.95	60.49	59.95	59.87	55.27	53.10	3.51
DHAT-AWP (Ours)	83.21	61.61	61.35	61.27	55.71	53.69	4.54
DHAT-CFA (Ours)	84.49	62.67	62.38	62.22	55.95	54.05	6.33

Architecture: WRN28-10		Attack ($\epsilon = 8/255$)					Robust Gap↓
CIFAR-100	Clean↑	PGD-10↑	PGD-20↑	PGD-50↑	C&W↑	AA↑	
MART [45]	54.69	32.06	31.90	31.88	28.77	27.25	9.96
AWP [49]	57.94	34.01	33.75	33.72	30.74	28.90	7.87
FSR [21]	57.48	32.93	32.30	32.26	29.16	27.04	7.84
CFA [47]	60.92	33.10	32.56	32.41	30.49	28.04	10.47
UIAT [9]	57.65	34.27	33.91	33.85	30.97	29.03	11.70
SGLR [27]	61.02	33.43	32.98	32.82	30.72	28.50	15.67
DHAT (Ours)	59.14	35.82	35.33	35.02	31.72	30.17	4.24
DHAT-AWP (Ours)	59.30	36.39	36.15	35.98	32.05	30.38	4.85
DHAT-CFA (Ours)	61.54	37.67	37.15	36.99	32.40	30.93	5.93

ImageNet dataset, we adopt the approach in [39] with 2-iteration PGD over 50 epochs, and set $\epsilon = 4/255$ and $\alpha = 1/255$ for adversarial perturbations. The hyperparameters λ_1 and λ_2 are set to 1.0 in all data sets. Comprehensive training details are available in the supplementary material.

4.1.3. Evaluation setup.

For robustness performance evaluation, we employ PGD [29], C&W [4], and AutoAttack (AA) [7] attacks under the ℓ_∞ norm. AutoAttack comprises APGD-DLR [7], APGD-CE [7], FAB [8], and Square [2]. “Clean” denotes natural examples without adversarial perturbations. Additionally, we introduce the concept of the robust generalization gap, referred to as the “Robust Gap”, which measures the difference in robustness performance between the training and test sets as a direct indicator of the generalization

ability [51]. This metric quantifies the strength of spurious correlations, where larger gaps indicate greater reliance on features that lack causal relationships with target labels.

4.2. Experimental Result

In this part, we conducted comprehensive evaluations of our proposed method across various visual datasets and compared it with mainstream adversarial training (AT) methods. Additionally, DHAT can be integrated with advanced AT strategies. The results are shown in Table 1.

4.2.1. Robust performance.

DHAT consistently demonstrates superior robustness across all datasets. For example, on CIFAR-10, DHAT outperforms the second-best method by 1.93% and 1.16% under PGD-10 and C&W attacks, respectively. DHAT also

Table 2. Comparison of robustness (%) and robust generalization gap (%). The **number** in bold indicates the best performance.

Dataset: CIFAR-10	ResNet-50			VGG-16			Inception-V3		
Method	Clean \uparrow	AA \uparrow	Robust Gap \downarrow	Clean \uparrow	AA \uparrow	Robust Gap \downarrow	Clean \uparrow	AA \uparrow	Robust Gap \downarrow
MART [45]	75.05	49.05	4.57	66.72	44.27	3.60	76.05	49.59	5.91
AWP [49]	75.59	50.80	3.91	67.14	45.97	3.47	76.74	50.46	4.07
FSR [21]	78.38	50.59	3.97	69.59	44.90	3.30	77.28	50.02	4.73
CFA [47]	77.88	50.64	4.27	70.45	45.53	4.66	76.70	49.97	4.46
UIAT [9]	78.42	51.00	2.99	68.46	45.27	3.57	75.19	51.23	3.70
SGLR [27]	80.39	50.55	5.21	70.90	45.04	3.94	80.62	50.73	5.00
DHAT (Ours)	79.94	51.92	1.85	70.01	46.40	1.34	77.85	51.81	1.92
DHAT-AWP (Ours)	76.84	52.05	2.34	67.41	47.21	2.18	77.12	52.08	2.88
DHAT-CFA (Ours)	80.97	52.38	2.09	70.52	47.83	2.21	78.52	52.67	2.44

shows the best performance on more complex datasets such as CIFAR-100 and high-resolution Imagenette datasets. Specifically, on ImageNet-1K, DHAT achieves improvements of 1.54% and 1.52% over the second-best method under PGD-10 and AA attacks, respectively.

4.2.2. Combine with other AT methods.

DHAT can be effectively combined with various AT methods to further enhance adversarial performance. Notably, DHAT can be combined with AWP and CFA, denoted as DHAT-AWP and DHAT-CFA, respectively. However, DHAT is not suitable for combining with methods that rely on spurious correlation to improve performance (*e.g.*, FSR, SLGR). In particular, DHAT-CFA achieves superior performance across all datasets. For instance, on Imagenette, DHAT-CFA provides a 2.84% performance improvement under the AA attack compared to the second-best method. Moreover, combining DHAT with advanced AT surpasses the performance of the original baseline methods in terms of both robustness and clean accuracy.

4.2.3. Robust overfitting.

Our method significantly reduces the robust generalization gap across all evaluated datasets, effectively mitigating the robust overfitting phenomenon. For example, on CIFAR-10, DHAT reduces the robust generalization gap by 4.41% and 6.01% compared to UIAT and MART, respectively. This reduction highlights DHAT’s ability to mitigate spurious correlation bias, thereby improving the model’s overall generalization performance. Detailed visualizations of the learning curve are provided in the supplementary material.

4.3. Generalization Analysis

In this part, we evaluate the generalizability of our proposed method by comprehensively evaluating its performance across various network architectures and under different magnitudes of adversarial attacks.

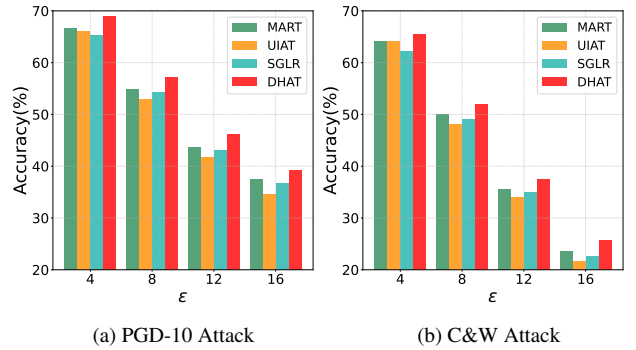


Figure 3. Comparisons of robustness (%) under varying ϵ adversarial attacks using ResNet-18 on CIFAR-10.

4.3.1. Performance with diverse network architecture.

To evaluate the adaptability of our method across different network architectures, we applied DHAT on ResNet-50, VGG-16, and Inception-V3. The performance comparisons are reported in Table 2. The results demonstrate the DHAT’s consistently superior robustness and generalization across a variety of model architectures. For example, DHAT-CFA outperforms the second-best method by 1.83% under AA attacks on ResNet-50. Similarly, on VGG-16, DHAT significantly reduces the robustness generalization gap by 1.96% compared to the second-best method.

4.3.2. Different attack magnitude.

Figure 3 illustrates the performance of DHAT under varying magnitudes of PGD-10 and C&W attacks. Our findings reveal that DHAT maintains a significant performance advantage across attack magnitudes. Compared to other methods, DHAT exhibits improved stability and robustness, with minimal performance degradation even under more severe attacks. This consistent performance across varying attack levels underscores the effectiveness of our approach in mitigating the impact of adversarial perturbations. Further details are provided in the supplementary material (Section 7).

Table 3. Comparison of computational costs (# A100 GPU hours) using different adversarial training methods on CIFAR-10.

Method	Architecture		
	ResNet-18	WRN28-10	Inception-V3
MART [45]	0.050	0.285	0.331
AWP [49]	0.048	0.274	0.318
FSR [21]	0.051	0.291	0.337
CFA [47]	0.045	0.262	0.303
UIAT [9]	0.040	0.245	0.283
SGLR [27]	0.039	0.240	0.278
DHAT (Ours)	0.041	0.248	0.287

Table 4. Comparison of robustness (%) and robust generalization gap (%). The **number** in bold indicates the best performance.

DHLR	FLOE	Clean \uparrow	PGD-10 \uparrow	AA \uparrow	Robust Gap \downarrow
		78.03	55.03	48.35	3.84
✓		78.79	56.56	49.47	1.98
	✓	78.50	56.22	49.73	2.06
✓	✓	79.28	57.21	50.25	0.81

4.4. Computational Efficiency

The computational costs of our method and baseline models are provided in terms of per-epoch training time on a single NVIDIA A100 GPU with a batch size of 128 on the CIFAR-10 dataset, as shown in Table 3. Our method demonstrates significantly improved time efficiency compared to the baseline MART, AWP, FSR, and CFA. While it requires slightly more computational resources than the state-of-the-art methods UIAT and SGLR, this minor increase is justifiable given the performance gains achieved.

4.5. Ablation Analysis

In this part, we conduct a comprehensive analysis of the impact of individual components and parameters of our model.

4.5.1. Impact of individual components.

We evaluate the contributions of the individual components of DHAT, specifically Debaised High-Confidence Logit Regularization (DHLR) and Foreground Logit Orthogonal Enhancement (FLOE), as shown in Table 4. The results indicate that both DHLR and FLOE significantly enhance model performance compared to the UIAT method. They enhance clean accuracy and adversarial robustness, while also reducing the gap in robustness generalization. This highlights the effectiveness of DHLR and FLOE in mitigating spurious correlation biases. Notably, the integration of both DHLR and FLOE results in a more substantial overall improvement in model performance.

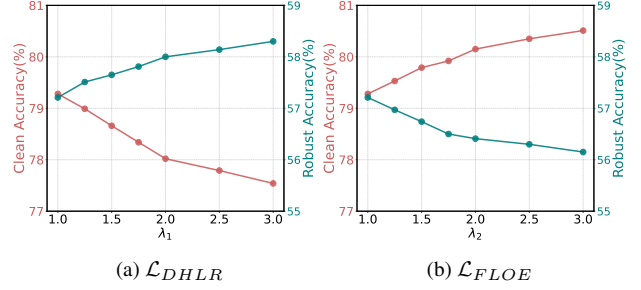


Figure 4. Analysis of hyper-parameters λ_1 and λ_2 using ResNet-18 on CIFAR-10. The robust accuracy denotes the accuracy under PGD-10 attack.

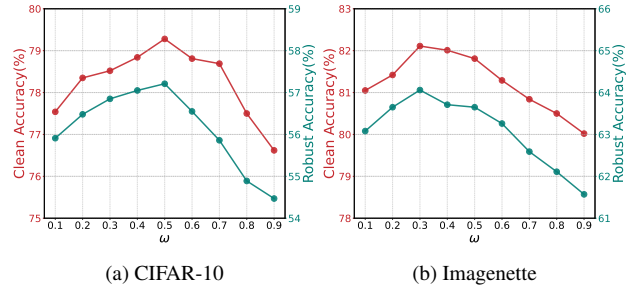


Figure 5. Analysis of hyper-parameters ω using ResNet-18 on CIFAR-10 and Imagenette. The robust accuracy denotes the accuracy under PGD-10 attack.

4.5.2. Analysis of parameter sensitivity.

Figure 4 illustrates the sensitivity of the optimization parameters λ_1 and λ_2 in DHAT. Our analysis reveals that these parameters influence the trade-off between adversarial robustness and clean accuracy. As λ_1 increases, adversarial robustness improves, while clean accuracy tends to decrease. This occurs because higher values of λ_1 increase the regularization strength, which enhances the alignment of adversarial example logits with debaised high-confidence logits. However, this stronger regularization effect may also lead to a reduced emphasis on clean accuracy, as the model focuses more on handling adversarial perturbations. Conversely, increasing λ_2 generally improves clean accuracy but may adversely affect adversarial robustness. Larger values of λ_2 help the model restore its attention to the normal state, which can result in less effective alignment of adversarial example logits with the debaised high-confidence logits.

4.5.3. Analysis of threshold factor for quantifying spurious bias.

Figure 5 illustrates the impact of threshold values w on datasets with varying resolutions. Our analysis reveals that as the threshold value increases, both clean accuracy and robustness initially improve before sharply declining. This initial improvement occurs because higher thresholds help

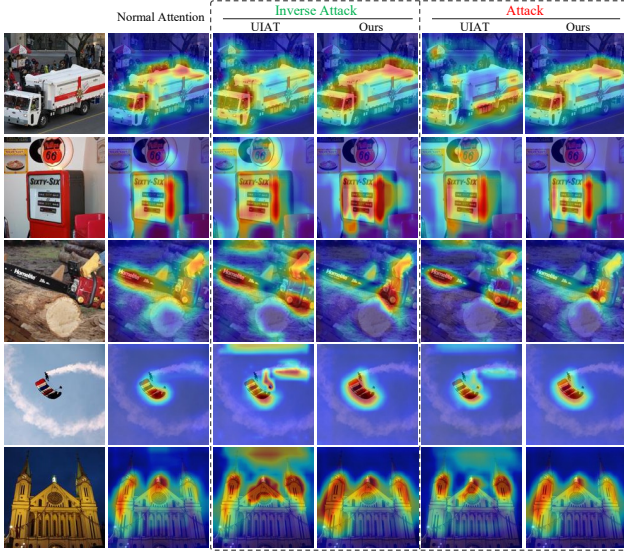


Figure 6. Visualization of feature activation maps using UIAT and DHAT, utilizing Grad-CAM under inverse attack ($\epsilon = -8$) and adversarial attack ($\epsilon = 8$). Left-to-right: the original image; normal feature activation maps; feature activation maps under adversarial attacks for UIAT and DHAT; and feature activation maps under inverse adversarial attacks for UIAT and DHAT.

in better separating accurate background features. However, further increasing the threshold eventually leads to the extraction of more foreground features, which causes significant performance degradation. For low-resolution datasets, the optimal threshold tends to be higher compared to high-resolution datasets, as high-resolution images more readily separate background features.

4.6. Discussion DHAT Effectiveness

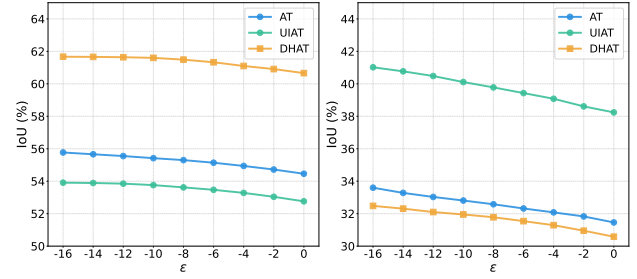
In this part, we analyze the mechanisms underlying the effectiveness of our proposed method, Debiased High-Confidence Adversarial Training (DHAT), with a focus on its capacity to mitigate spurious correlation bias.

4.6.1. Feature Activation Map Analysis

Figure 6 visualizes feature activation maps of UIAT and DHAT models under adversarial and inverse adversarial attacks. DHAT successfully maintains normal attention patterns, while UIAT exhibits biased activation with attention shifting significantly to background features during inverse attacks. DHAT achieves this robust performance by recalibrating biased high-confidence logits and systematically reducing correlation between logits and background features.

4.6.2. Quantitative Evaluation of Bias Mitigation

Figure 7 quantifies DHAT’s effectiveness through IoU between attention maps and true foreground/background regions. DHAT achieves higher foreground IoU and lower background IoU than both AT and UIAT, confirming its



(a) IoU with Normal Foreground (b) IoU with Normal Background

Figure 7. IoU of attention regions with normal foreground and background regions. The comparison is conducted among conventional AT, UIAT, and DHAT on the Imagenette Dataset.

Table 5. Comparison of training with different magnitude reverse adversarial samples (UIAT) and our debiased training DHAT using WRN28-10 on the CIFAR-10.

Method	ϵ of \hat{z}	Training Set		Test Set		Robust Gap↓
		PGD-10↑	AA↑	PGD-10↑	AA↑	
UIAT	-4	90.53	61.45	82.94	52.07	9.38
UIAT	-8	92.57	62.87	82.26	51.33	11.54
UIAT	-12	94.90	65.28	81.72	50.85	14.43
DHAT (ours)	-4	88.73	56.61	83.95	53.10	3.51

superior feature attention. Table 5 shows stronger inverse attacks in UIAT worsen overfitting, increasing the robust gap from 9.38 to 14.43. In contrast, DHAT achieves better test robustness (83.95% PGD-10, 53.10% AA) with a significantly smaller robust gap (3.51), effectively mitigating overfitting while maintaining strong performance.

5. Conclusion

In this work, we identify a critical issue in adversarial training: AT model exhibits biased feature activation under inverse adversarial attacks. Specifically, training with inverse adversarial examples causes the model attention to shift from the foreground to background features, resulting in spurious correlation bias. To tackle this challenge, we propose a novel method called Debiased High-Confidence Adversarial Training (DHAT). DHAT incorporates two pivotal techniques: Debiased High-Confidence Logit Regularization (DHLR) and Foreground Logit Orthogonal Enhancement (FLOE). DHLR quantifies the bias towards background feature activation and recalibrates biased high-confidence logits to align the logits of adversarial examples with these debiased high-confidence logits. FLOE further restores the model’s attention to its normal state by reducing the correlation between high-confidence logits and background features in affine space. This work highlights DHAT’s effectiveness in enhancing model resilience and presents an adversarial training framework that integrates seamlessly with advanced training strategies.

Acknowledgment

This work is supported by the National Natural Science Foundation of China under Grant No. 62276221, 62376232; Key Laboratory of Equipment Data Security and Guarantee Technology, Ministry of Education under Grant No. 2024020200.

References

- [1] Ola Ahmad, Nicolas B  reux, Lo  c Baret, Vahid Hashemi, and Freddy Lecue. Causal analysis for robust interpretability of neural networks. In *WAVC*, pages 4685–4694, 2024. 2
- [2] Maksym Andriushchenko, Francesco Croce, Nicolas Flammarion, and Matthias Hein. Square attack: a query-efficient black-box adversarial attack via random search. In *ECCV*, 2020. 5, 11
- [3] Saeid Asgari, Aliasghar Khani, Fereshte Khani, Ali Gholami, Linh Tran, Ali Mahdavi Amiri, and Ghassan Hamarneh. Masktune: Mitigating spurious correlations by forcing to explore. In *NeurIPS*, 2022. 1
- [4] Nicholas Carlini and David Wagner. Towards evaluating the robustness of neural networks. *IEEE Symp. Security Privacy*, pages 39–57, 2017. 3, 5, 11
- [5] Hyuna Cho, Yubin Han, and Won Hwa Kim. Anti-adversarial consistency regularization for data augmentation: Applications to robust medical image segmentation. In *MI-CAI*, 2023. 1
- [6] Jonathan Crabb   and Mihaela van der Schaar. Evaluating the robustness of interpretability methods through explanation invariance and equivariance. In *NeurIPS*, 2023. 2
- [7] Francesco Croce and Matthias Hein. Reliable evaluation of adversarial robustness with an ensemble of diverse parameter-free attacks. In *ICML*, 2020. 3, 5, 11
- [8] Francesco Croce and Matthias Hein. Minimally distorted adversarial examples with a fast adaptive boundary attack. In *ICML*, 2020. 5, 11
- [9] Junhao Dong, Seyed-Mohsen Moosavi-Dezfooli, Jianhuang Lai, and Xiaohua Xie. The enemy of my enemy is my friend: Exploring inverse adversaries for improving adversarial training. In *CVPR*, 2023. 1, 2, 3, 5, 6, 7, 11, 12, 13, 14
- [10] Xiaoyi Dong, Jiangfan Han, Dongdong Chen, Jiayang Liu, Huanyu Bian, Zehua Ma, Hongsheng Li, Xiaogang Wang, Weiming Zhang, and Nenghai Yu. Robust superpixel-guided attentional adversarial attack. In *CVPR*, 2020. 2, 4
- [11] Alhussein Fawzi, Hamza Fawzi, and Omar Fawzi. Adversarial vulnerability for any classifier. In *NeurIPS*, 2018. 1
- [12] Liam Fowl, Micah Goldblum, Ping-yeh Chiang, Jonas Geiping, Wojciech Czaja, and Tom Goldstein. Adversarial examples make strong poisons. In *NeurIPS*, 2021. 3
- [13] Shengyi Gao, Zhe Chen, Guo Chen, Wenhai Wang, and Tong Lu. Avsegformer: Audio-visual segmentation with transformer. In *AAAI*, 2024. 1
- [14] Ian J Goodfellow, Jonathon Shlens, and Christian Szegedy. Explaining and harnessing adversarial examples. *arXiv preprint arXiv:1412.6572*, 2014. 1, 2
- [15] Xinzhe Han, Shuhui Wang, Chi Su, Qingming Huang, and Qi Tian. General greedy de-bias learning. *IEEE TPAMI*, 45 (8):9789–9805, 2023. 2
- [16] Kaiming He, Xiangyu Zhang, Shaoqing Ren, and Jian Sun. Deep residual learning for image recognition. In *CVPR*, 2016. 4
- [17] Jonathan Ho, Ajay Jain, and Pieter Abbeel. Denoising diffusion probabilistic models. *NeurIPS*, 2020. 12
- [18] FastAI Jeremy Howard. Imagenette: A smaller subset of imagenet. In *Github*. <https://github.com/fastai/imagenette>, 2019. 2
- [19] Zhichao Huang, Yanbo Fan, Chen Liu, Weizhong Zhang, Yong Zhang, Mathieu Salzmann, Sabine S  sstrunk, and Jue Wang. Fast adversarial training with adaptive step size. *IEEE TIP*, 32:6102–6114, 2023. 1
- [20] Pavel Izmailov, Polina Kirichenko, Nate Gruver, and Andrew G Wilson. On feature learning in the presence of spurious correlations. In *NeurIPS*, 2022. 2
- [21] Woo Jae Kim, Yoonki Cho, Junsik Jung, and Sung-Eui Yoon. Feature separation and recalibration for adversarial robustness. In *CVPR*, 2023. 3, 5, 6, 7, 13
- [22] Alexander Kirillov, Eric Mintun, Nikhila Ravi, Hanzi Mao, Chloe Rolland, Laura Gustafson, Tete Xiao, Spencer Whitehead, Alexander C Berg, Wan-Yen Lo, et al. Segment anything. In *ICCV*, 2023. 4, 11, 13, 14
- [23] Alex Krizhevsky, Geoffrey Hinton, et al. Learning multiple layers of features from tiny images. In *Toronto, ON, Canada*, 2009. 4, 11
- [24] Boqi Li and Weiwei Liu. Wat: improve the worst-class robustness in adversarial training. In *AAAI*, 2023. 1
- [25] Bo Li, Haoke Xiao, and Lv Tang. Asam: Boosting segment anything model with adversarial tuning. In *CVPR*, 2024. 1
- [26] Feng Li, Qing Jiang, Hao Zhang, Tianhe Ren, Shilong Liu, Xueyan Zou, Huaizhe Xu, Hongyang Li, Jianwei Yang, Chunyuan Li, et al. Visual in-context prompting. In *CVPR*, 2024. 1
- [27] Zhuorong Li, Daiwei Yu, Lina Wei, Canghong Jin, Yun Zhang, and Sixian Chan. Soften to defend: Towards adversarial robustness via self-guided label refinement. In *CVPR*, 2024. 3, 5, 6, 7, 13, 14
- [28] Ye Liu, Yaya Cheng, Lianli Gao, Xianglong Liu, Qilong Zhang, and Jingkuan Song. Practical evaluation of adversarial robustness via adaptive auto attack. In *CVPR*, 2022. 13
- [29] Aleksander Madry, Aleksandar Makelov, Ludwig Schmidt, Dimitris Tsipras, and Adrian Vladu. Towards deep learning models resistant to adversarial attacks. In *ICLR*, 2018. 2, 5, 11
- [30] Yifei Ming, Hang Yin, and Yixuan Li. On the impact of spurious correlation for out-of-distribution detection. In *AAAI*, 2022. 1
- [31] Olga Russakovsky, Jia Deng, Hao Su, Jonathan Krause, Sanjeev Satheesh, Sean Ma, Zhiheng Huang, Andrej Karpathy, Aditya Khosla, Michael Bernstein, et al. Imagenet large scale visual recognition challenge. *IJCV*, 115:211–252, 2015. 4

- [32] Hadi Salman, Andrew Ilyas, Logan Engstrom, Sai Vemprala, Aleksander Madry, and Ashish Kapoor. Unadversarial examples: Designing objects for robust vision. In *NeurIPS*, 2021. 1, 3
- [33] Ramprasaath R Selvaraju, Michael Cogswell, Abhishek Das, Ramakrishna Vedantam, Devi Parikh, and Dhruv Batra. Grad-cam: Visual explanations from deep networks via gradient-based localization. In *ICCV*, 2017. 4, 13
- [34] Ramprasaath R Selvaraju, Michael Cogswell, Abhishek Das, Ramakrishna Vedantam, Devi Parikh, and Dhruv Batra. Grad-cam: Visual explanations from deep networks via gradient-based localization. In *CVPR*, 2017. 1
- [35] Seonguk Seo, Joon-Young Lee, and Bohyung Han. Information-theoretic bias reduction via causal view of spurious correlation. In *AAAI*, 2022. 1
- [36] Ali Shafahi, Mahyar Najibi, Mohammad Amin Ghiasi, Zheng Xu, John Dickerson, Christoph Studer, Larry S Davis, Gavin Taylor, and Tom Goldstein. Adversarial training for free! In *NeurIPS*, 2019. 1
- [37] Kele Shao, Keda Tao, Can Qin, Haoxuan You, Yang Sui, and Huan Wang. Holitom: Holistic token merging for fast video large language models. *arXiv preprint arXiv:2505.21334*, 2025. 1
- [38] Karen Simonyan and Andrew Zisserman. Very deep convolutional networks for large-scale image recognition. *arXiv preprint arXiv:1409.1556*, 2014. 4
- [39] Naman Deep Singh, Francesco Croce, and Matthias Hein. Revisiting adversarial training for imagenet: Architectures, training and generalization across threat models. In *NeurIPS*, 2023. 5, 11
- [40] Ajay Subramanian, Elena Sizikova, Najib Majaj, and Denis Pelli. Spatial-frequency channels, shape bias, and adversarial robustness. In *NeurIPS*, 2024. 1
- [41] Mukund Sundararajan, Ankur Taly, and Qiqi Yan. Axiomatic attribution for deep networks. In *ICML*, 2017. 13
- [42] Christian Szegedy, Wojciech Zaremba, Ilya Sutskever, Joan Bruna, Dumitru Erhan, Ian Goodfellow, and Rob Fergus. Intriguing properties of neural networks. In *ICLR*, 2014. 1
- [43] Christian Szegedy, Wei Liu, Yangqing Jia, Pierre Sermanet, Scott Reed, Dragomir Anguelov, Dumitru Erhan, Vincent Vanhoucke, and Andrew Rabinovich. Going deeper with convolutions. In *CVPR*, 2015. 4
- [44] Xinlong Wang, Tao Kong, Chunhua Shen, Yuning Jiang, and Lei Li. Solo: Segmenting objects by locations. In *ECCV*, 2020. 13, 14
- [45] Yisen Wang, Difan Zou, Jinfeng Yi, James Bailey, Xingjun Ma, and Quanquan Gu. Improving adversarial robustness requires revisiting misclassified examples. In *ICLR*, 2020. 1, 3, 5, 6, 7, 13, 14
- [46] Zekai Wang, Tianyu Pang, Chao Du, Min Lin, Weiwei Liu, and Shuicheng Yan. Better diffusion models further improve adversarial training. In *ICML*, 2023. 13
- [47] Zeming Wei, Yifei Wang, Yiwen Guo, and Yisen Wang. Cfa: Class-wise calibrated fair adversarial training. In *CVPR*, 2023. 3, 5, 6, 7, 13
- [48] Jing Wen, Siu-Ming Yiu, and Lucas CK Hui. Defending against model inversion attack by adversarial examples. In *IEEE CSR*, pages 551–556, 2021. 2
- [49] Dongxian Wu, Shu-Tao Xia, and Yisen Wang. Adversarial weight perturbation helps robust generalization. In *NeurIPS*, 2020. 3, 5, 6, 7, 13
- [50] Cihang Xie, Mingxing Tan, Boqing Gong, Jiang Wang, Alan L Yuille, and Quoc V Le. Adversarial examples improve image recognition. In *CVPR*, 2020. 3
- [51] Shenglin Yin, Kelu Yao, Sheng Shi, Yangzhou Du, and Zhen Xiao. Again: Adversarial training with attribution span enlargement and hybrid feature fusion. In *CVPR*, 2023. 5, 11
- [52] Sergey Zagoruyko and Nikos Komodakis. Wide residual networks. *arXiv preprint arXiv:1605.07146*, 2016. 4
- [53] Bohan Zeng, Shanglin Li, Xuhui Liu, Sicheng Gao, Xiaolong Jiang, Xu Tang, Yao Hu, Jianzhuang Liu, and Baochang Zhang. Controllable mind visual diffusion model. In *AAAI*, 2024. 1
- [54] Hongyang Zhang, Yaodong Yu, Jiantao Jiao, Eric Xing, Laurent El Ghaoui, and Michael Jordan. Theoretically principled trade-off between robustness and accuracy. In *ICML*, 2019. 1
- [55] Tianren Zhang, Chujie Zhao, Guanyu Chen, Yizhou Jiang, and Feng Chen. Feature contamination: Neural networks learn uncorrelated features and fail to generalize. In *ICML*, 2024. 2

Supplementary Materials

This supplementary material offers a detailed examination of the methodologies and results that underpin the experiments in our study. It is designed to provide comprehensive information to validate the findings and ensure reproducibility and transparency.

The content is organized as follows:

- **Section 6:** A comprehensive and detailed description of the experimental setup and methodology.
- **Section 7:** A formal presentation of the proposed algorithm, including its pseudocode representation.
- **Section 8:** In-depth evaluation of model performance under various transfer attack scenarios.
- **Section 9:** Detailed results from adversarial training using synthetic data for robustness assessment.
- **Section 10:** Extensive exploration of techniques for generating foreground-background attention maps.
- **Section 11:** Thorough examination of the model’s robustness under varying levels of attack intensity.

6. Experimentation Details

In this part, we provide a comprehensive overview of the experimental setup.

6.1. Training Setup

6.1.1. CIFAR-10 and CIFAR-100

For the CIFAR-10 and CIFAR-100 [23] datasets, we employ the Stochastic Gradient Descent (SGD) optimizer with a momentum of 0.9 and a weight decay factor of 5×10^{-4} . The initial learning rate is set to 0.1, and models undergo 100 epochs of training with the learning rate reduced by a factor of 0.1 at the 80th and 90th epochs.

For adversarial training on these datasets, we create adversarial examples through a 10-iteration attack where the maximum ℓ_∞ -norm of the adversarial perturbation is limited to $\epsilon = 8/255$, using a step size of $\alpha = 2/255$. To ensure reliability and fairness, we align the inverse adversarial example generation process with the UIAT settings [9], employing the same loss function and perturbation constrained by $\epsilon = 4/255$.

6.1.2. ImageNet-1K

For the ImageNet-1K dataset, we strictly follow the training protocol established in [39] to ensure fair comparison with existing methods. Specifically, we implement a 2-iteration PGD over 50 epochs, and set $\epsilon = 4/255$ and $\alpha = 1/255$ for adversarial perturbations. This adherence to established benchmarking parameters enables direct and meaningful comparison with state-of-the-art approaches evaluated on this challenging large-scale dataset.

6.1.3. Common Settings

The hyperparameters λ_1 and λ_2 are consistently set to 1.0 across all datasets. To maintain experimental fairness, all comparative methods undergo identical training strategies with the same number of epochs and optimizer configurations. For Grad-CAM to quantify the spurious correlation bias, we use a pre-trained ResNet-18 model under simple training, introducing minimal additional training cost.

All experiments were conducted on a single NVIDIA Tesla A100. Notably, our method does not employ label smoothing techniques to avoid potential conflicts with efforts to mitigate spurious correlation bias, as label smoothing can blur class boundaries and undermine the precision required for robust decision-making. Additionally, unlike UIAT, our approach does not utilize momentum terms to stabilize the generation process of inverse adversarial examples, instead focusing solely on the intrinsic properties and underlying dynamics of our method. Comprehensive training details are available in the supplementary material.

6.2. Evaluation Setup

Our evaluation consists of two main components: robustness performance and robust generalization. To evaluate robustness performance, we use PGD [29], C&W [4], and AutoAttack (AA) [7] within the ℓ_∞ -norm. AutoAttack includes several attack methods such as APGD-DLR [7], APGD-CE [7], FAB [8], and Square [2]. Adversarial attacks are generated using a step size of $\alpha = 2/255$ and a specified maximum ℓ_∞ -norm. Note that “Clean” indicates natural examples unaffected by adversarial perturbations.

To evaluate robust generalization, we introduce the concept of the robust generalization gap [51] denoted as the “Robust Gap” quantifying the difference in robust performance between training and test sets under adversarial attacks. A smaller robust gap indicates improved robust generalization, reflecting reduced vulnerability to robust overfitting in the adversarial training model.

7. Algorithm Details

Algorithm 1 outlines the complete workflow of our proposed *Debiased High-Confidence Adversarial Training* (DHAT) framework, which systematically mitigates spurious correlations in adversarial training through two primary components: Debiased High-Confidence Logit Regularization (DHLR) and Foreground Logit Orthogonal Enhancement (FLOE).

To efficiently compute attention maps, we employ Grad-CAM (Line 11) due to its computational efficiency. However, our framework is compatible with alternative saliency-based methods, such as SAM [22], which can provide enhanced performance at a higher computational cost. The extraction of background features (Lines 13-14) is performed

Algorithm 1 Debiased High-Confidence Adversarial Training (DHAT)

Require: Training dataset $(X, Y) = \{(x_i, y_i)\}_{i=1}^N$; Network parameters θ ; Perturbation budget ϵ ; Hyperparameters λ_1, λ_2 ; Attention threshold ω .

Ensure: Robust model parameters θ^*

```
1: Initialize network parameters  $\theta$ 
2: for each epoch do
3:   for each mini-batch  $(x, y)$  do
4:     // Generate adversarial examples
5:      $\hat{x} \leftarrow \arg \max_{\|x' - x\|_p \leq \epsilon} \mathcal{L}_{AT}(f_\theta(x'), y)$ 
6:      $\hat{z} \leftarrow f_\theta(\hat{x})$ 
7:     // Generate inverse adversarial examples
8:      $\tilde{x} \leftarrow \arg \min_{\|x' - x\|_p \leq \epsilon} \mathcal{L}_{Inv}(f_\theta(x'), y)$ 
9:      $\tilde{z} \leftarrow f_\theta(\tilde{x})$ 
10:    // Compute attention maps using a selected method
     $\mathcal{A} \in \{\text{Grad-CAM, Integrated-Grad, SAM, etc.}\}$ 
11:     $M \leftarrow \mathcal{A}(x)$  {Different attention map computation techniques}
12:    // Extract background features from inverse adversarial examples
13:     $[\tilde{x}_{(B)}]_{(i,j)} \leftarrow \mathbb{I}_{(M_{i,j} < \omega)} \cdot \tilde{x}_{(i,j)}$ 
14:     $\tilde{z}_{(B)} \leftarrow f_\theta(\tilde{x}_{(B)})$ 
15:    // Compute debiased high-confidence logits
16:     $\tilde{z}^* \leftarrow \tilde{z} - \tilde{z}_{(B)}$ 
17:    // Compute DHLR loss
18:     $\mathcal{L}_{DHLR} \leftarrow \mathcal{L}_{KL}(\phi(\tilde{z}^*) || \phi(\tilde{z}))$ 
19:    // Compute FLOE loss
20:     $\mathcal{L}_{FLOE} \leftarrow -|\tilde{z} - \frac{\tilde{z} \cdot \tilde{z}_{(B)}}{|\tilde{z}_{(B)}|^2} \cdot \tilde{z}_{(B)}|_p$ 
21:    // Compute total loss
22:     $\mathcal{L}_{DHAT} \leftarrow \mathcal{L}_{AT}(\hat{z}, y) + \lambda_1 \cdot \mathcal{L}_{DHLR} + \lambda_2 \cdot \mathcal{L}_{FLOE}$ 
23:    // Update network parameters
24:     $\theta^* \leftarrow \theta - \nabla_\theta \mathcal{L}_{DHAT}$ 
25:  end for
26: end for
27: return  $\theta^*$ 
```

using an adaptive threshold ω , ensuring the identification of non-discriminative regions that contribute to spurious correlations. The overall training objective (Line 23) integrates standard adversarial training with our proposed debiasing regularization terms, weighted by λ_1 and λ_2 .

Despite incorporating additional minimal computational steps, the DHAT framework introduces only a marginal increase in resource consumption compared to standard adversarial training while significantly enhancing model robustness. Crucially, DHAT achieves these improvements without compromising clean-data accuracy, making it a highly practical and scalable solution for real-world adversarial defense applications.

8. Performance Under Transfer Attack

In this part, we evaluate our proposed model’s performance under transfer attacks and compare it with the UIAT [9]. Transfer attacks evaluate a model’s robustness by testing its performance against adversarial examples generated from different source models, which simulate real-world conditions where attackers may use varied strategies. This testing is essential to ensure that a model’s adversarial defenses generalize effectively beyond its training environment and are robust against diverse attack methods. By evaluating the performance under transfer attacks, we ensure that our model is robust not only to attacks generated by its own architecture but also to those from different models, providing a more comprehensive measure of robustness.

Table 6 presents the robust accuracy of various models under transfer attacks with an ℓ_∞ -norm perturbation of $\epsilon = 8$. The table compares the performance of the UIAT method with that of our proposed model across different target models and transfer attack types.

8.1. Robustness Performance

Our model consistently outperforms UIAT across all transfer adversarial attacks and target models. For example, when the WRN28-10 model is trained with our proposed DHAT and subjected to AA attacks generated from ResNet-50, VGG16, and Inc-V3 source models, the defense success rate improves by 1.21%, 1.14%, and 1.44% compared to UIAT, respectively. This demonstrates the model’s robustness, highlighting its effectiveness not only in specific attack scenarios but also across various model architectures.

8.2. Robustness Across Various Attack Types

Our proposed model DHAT demonstrates enhanced robustness, particularly against more challenging attacks such as PGD-50 and C&W. For instance, when using the ResNet-18 as the source model, our method achieves improvements of up to 1.88% and 2.39% under PGD-50 and C&W attacks from WRN28-10, respectively, compared to UIAT. This highlights the model’s superior capability to withstand adversarial perturbations.

8.3. Generalization Across Various Source Models

Our model exhibits strong performance across a range of source models, including VGG-16, WRN28-10, and ResNet-18. This indicates that the improved robustness of our model is not limited to specific attacks generated from source architectures but generalizes effectively across different adversarial settings.

9. Performance with Generated Data

We employ Diffusion Denoising Probabilistic Models (DDPM) [17] to generate an additional 50K samples for

Table 6. Transfer attack accuracy (%) in the single-model transfer scenario. The **number** in bold indicates the best accuracy.

Attack ($\epsilon = 8$)	Performance of UIAT / DHAT								
	Target: VGG-16			Target: WRN28-10			Target: ResNet-18		
	\Rightarrow ResNet-50	\Rightarrow Inc-V3	\Rightarrow WRN28-10	\Rightarrow ResNet-50	\Rightarrow VGG16	\Rightarrow Inc-v3	\Rightarrow WRN28-10	\Rightarrow VGG16	\Rightarrow Inc-v3
FGSM	63.42/ 64.83	63.44/ 64.51	63.73/ 64.88	77.11/ 78.73	78.08/ 79.27	77.84/ 78.69	73.01/ 74.80	74.00/ 75.03	72.43/ 73.18
PGD-10	53.09/ 54.46	52.81/ 53.96	54.17/ 55.36	61.93/ 62.87	64.73/ 65.70	61.40/ 62.56	58.56/ 60.30	59.91/ 60.89	57.82/ 58.75
PGD-20	52.73/ 54.25	52.63/ 53.70	53.80/ 55.29	61.52/ 62.68	64.60/ 65.65	61.19/ 62.38	58.13/ 60.04	59.80/ 60.78	57.48/ 58.42
PGD-50	52.68/ 54.25	52.62/ 53.67	53.77/ 55.27	61.51/ 62.65	64.56/ 65.68	61.17/ 62.24	58.15/ 60.03	59.78/ 60.83	57.45/ 58.46
C&W	51.90/ 53.44	51.38/ 52.61	55.31/ 56.35	61.05/ 62.02	63.32/ 64.40	60.76/ 61.98	57.73/ 60.12	57.44/ 58.74	57.71/ 59.25
AA	56.31/ 57.94	56.02/ 56.98	59.65/ 60.77	67.18/ 68.39	71.86/ 73.00	64.39/ 65.83	62.36/ 63.19	65.19/ 66.07	60.69/ 61.94

Table 7. Comparison of robustness (%) and robust generalization gap (%) for models trained on generated data. The **bolded numbers** indicate the best performance.

CIFAR-10	ResNet-18			WRN28-10		
	Clean \uparrow	AA \uparrow	Robust Gap \downarrow	Clean \uparrow	AA \uparrow	Robust Gap \downarrow
MART [45]	83.45	49.45	2.91	84.26	51.95	8.73
AWP [49]	83.78	50.79	2.03	84.10	53.29	6.11
FSR [21]	83.19	50.53	2.35	83.88	53.03	7.05
CFA [47]	84.97	50.85	2.98	85.81	53.35	8.94
UIAT [9]	85.10	52.09	3.04	86.73	54.59	9.41
SGLR [27]	86.35	51.27	2.75	87.72	53.77	11.25
DHAT (Ours)	87.62	54.42	0.83	88.94	56.92	2.48

CIFAR-100	ResNet-18			WRN28-10		
	Clean \uparrow	AA \uparrow	Robust Gap \downarrow	Clean \uparrow	AA \uparrow	Robust Gap \downarrow
MART [45]	54.73	27.70	2.88	55.87	30.20	8.86
AWP [49]	57.55	29.33	2.37	59.71	31.83	7.13
FSR [21]	58.10	28.94	2.47	59.03	30.44	7.40
CFA [47]	60.13	28.85	3.01	61.56	29.61	9.13
UIAT [9]	59.92	28.48	4.47	60.24	30.98	14.32
SGLR [27]	61.25	29.10	4.15	62.39	30.15	17.05
DHAT (Ours)	63.14	32.21	0.98	64.80	34.71	2.96

both CIFAR-10 and CIFAR-100 datasets following the [46]. This synthetic data is then used to augment the training of both our method and all baseline models. The performance comparisons, as shown in Table 7, illustrate the impact of additional data on robustness and generalization.

9.1. Robustness Performance

The results in Table 7 demonstrate that our method outperforms baseline methods in terms of robustness when trained with the additional synthetic data. This improvement highlights the effectiveness of our approach in leveraging extra data to enhance model robustness, particularly under adversarial conditions.

9.2. Generalization Performance

We observe that, compared to the results in Table 1, most models trained with the additional data exhibit a reduced Robust Gap, indicating improved generalization. However, both UIAT and SGLR exhibit limited improvements in robust generalization. These methods rely on spurious correlations during training, which hinders their generalization

Table 8. Comparison of robustness (%) and robust generalization gap (%) for using various attention map generation techniques using WRN28-10 on the CIFAR-10.

Method	Clean \uparrow	PGD-10 \uparrow	C&W \uparrow	AA \uparrow	Robust Gap \downarrow
-	82.94	58.66	54.11	52.17	7.92
Grad-CAM [33]	83.95	60.49	55.27	53.10	3.51
Integrated-Grad [41]	83.97	60.35	55.18	53.04	3.68
SOLO [44]	84.26	61.60	56.74	54.93	3.09
SAM [22]	85.65	62.44	58.10	56.38	2.46

performance even with the added data. Although UIAT and SGLR benefit from enhanced robustness due to increased data diversity, their robust generalization remains suboptimal, likely due to their dependence on non-essential features. This finding underscores the unique advantage of our method in achieving both robust accuracy and generalization with enriched datasets.

10. Impact of Foreground-Background Recognition Techniques

In this part, we investigate the influence of different attention map generation techniques on the performance of De-biased High-Confidence Logit Regularization (DHAT), as seen in Table 8. Our exploration extends beyond the initially employed Grad-CAM method to encompass a variety of attention map generation approaches, thereby providing a comprehensive analysis of their effects on model robustness and generalization.

10.1. Exploration of Various Attention Map

The primary approach detailed in the main text utilizes Grad-CAM [33], a widely adopted method in weakly supervised object segmentation [28], to extract foreground and background feature maps efficiently. Grad-CAM offers a balance between computational efficiency and effectiveness, making it suitable for large-scale evaluations. However, to understand the broader applicability and potential improvements, we incorporated additional attention map generation techniques, including Integrated Gradients [41],

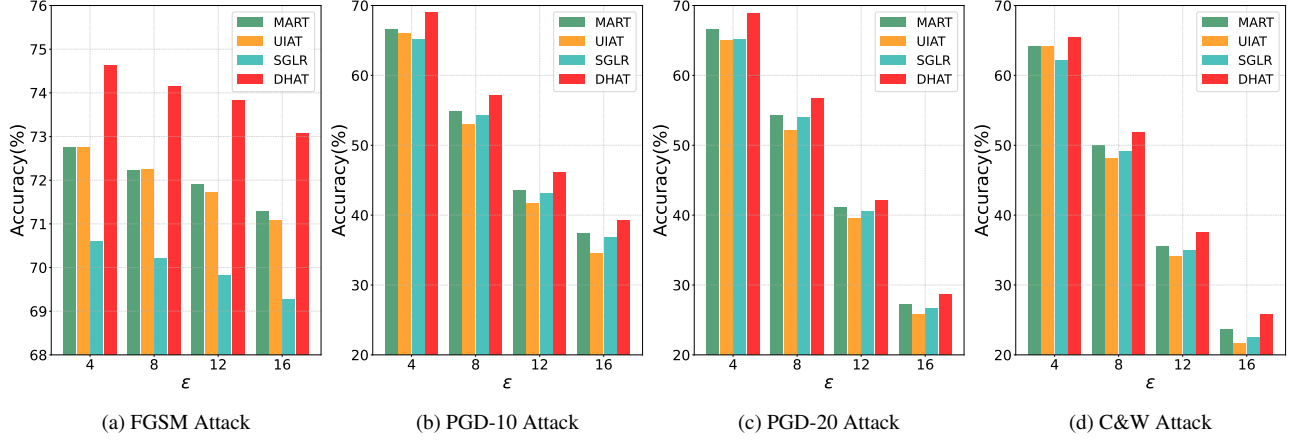


Figure 8. Comparisons with varying ϵ values using ResNet-18 on the CIFAR-10. The x -axis represents the ϵ value, while y -axis represents the robust accuracy (%).

SOLO [44], and SAM [22].

10.2. Evaluation of Advanced Attention Map Models

Incorporating more sophisticated attention map generation models, such as SAM, demonstrated enhanced robustness and reduced robust generalization gaps compared to simpler methods like Grad-CAM. These advanced models provide finer and more accurate segmentation of foreground and background features, which in turn leads to better alignment of high-confidence logits under adversarial conditions. However, this improvement in performance comes at the cost of increased computational overhead. More complex models require greater processing power and longer training times, which may be a limiting factor in resource-constrained environments.

10.3. Trade-Off Between Performance and Computational Efficiency

While the adoption of advanced attention map techniques can yield superior performance metrics, researchers must consider the trade-offs involved. Enhanced models may offer marginal gains in robustness and generalization, but the additional computational resources and time required may not always justify these benefits, especially in applications where real-time processing is essential. Therefore, the choice of attention map generation technique should be informed by the specific requirements and constraints of the deployment scenario.

11. Robustness under Various Magnitude Attacks

In this part, we evaluate the robustness of our proposed model under various levels of adversarial perturbations, quantified by different ϵ values. We compare our model

with two baseline methods, MART [45] and UIAT [9], and the state-of-the-art SGLR method [27] across various attack types, including FGSM, PGD-10, PGD-20, and C&W. We aim to demonstrate the superior generalization and robustness of our model under progressively challenging adversarial conditions. Figure 8 shows the accuracy of different methods under various ϵ values for each attack type.

The comparative analysis of our model with MART, UIAT, and SGLR reveals several key insights:

11.1. Robustness Across Various Attack Types

Our model consistently outperforms the baselines and SGLR across all attack types and ϵ values. This consistent superiority underscores our model’s robust generalization ability, allowing it to maintain high accuracy even under more challenging adversarial attack conditions.

11.2. Generalization Against Various Attacks

The results suggest that the defensive mechanisms in our model are highly effective in mitigating the impact of various adversarial attacks (*i.e.*, FGSM, PGD-10, PGD-20, C&W). This robustness is especially evident in scenarios with stronger attacks and higher ϵ values, where our model shows superior performance compared to existing methods.

11.3. Practical Applicability

The enhanced robustness of our model across different ϵ values and attack types demonstrates its practical applicability in real-world scenarios, where adversarial perturbations can vary in strength and sophistication.